Characterizing Low-Data-Rate Power Line Communication Channels

Adedayo O. Aderibole, Erik K. Saathoff, *Graduate Student Member, IEEE*, Kevin J. Kircher, *Member, IEEE*, Aaron W. Langham, *Graduate Student Member, IEEE*, Leslie K. Norford, and Steven B. Leeb, *Fellow, IEEE*

***Abstract*— Electric power lines could, in principle, provide a ubiquitous wired communication network linking electrical loads, power meters, and other devices. This communication infrastructure could unlock new sensing and control capabilities, improving the efficiency and reliability of power system operations. In practice, however, power line communication (PLC) is complicated by both known and variable difficulties related to background noise, signal attenuation, and unknown line impedances. This article develops instrumentation that characterizes and verifies line characteristics for PLC applications, especially for demand response and control applications. This instrumentation provides a window to key variables that affect communication on a local power distribution network. With these measurements, limits on PLC communication can be verified before an installation, and a PLC system may also be adaptively tuned to measurements of the current local environment. Field experiments in a challenging microgrid and a 24-floor apartment building demonstrate an appropriately tailored PLC system communicating reliably in locations where conventional PLC fails.**

***Index Terms*— Attenuation, impedance, microgrid, noise, power line communication (PLC).**

I. Value of Measurements in PLC

MANY energy distribution and smart grid applications, such as coordinating electrical loads and remotely collecting power meter data, demand reliable communication. The design of communication and control systems for energy applications present unique challenges and opportunities. Distribution systems limit energy delivery performance. On microgrids for mission critical applications or emergency use, generation may limit the performance of the grid. However, even when energy is relatively plentiful in principle, distribution components like transformers may respond poorly to peak loading, e.g., a collection of air conditioners running on a hot day in a high-rise apartment building. Low-bandwidth communication strategies are more than adequate in many cases for exchanging the small packets of data necessary for coordinating load demand response on a smart grid [1], [2]. Local data exchange, rather than the IoT-style client-server model, also reduces security risk [2].

Existing power lines are a natural choice of communication channel for smart grid applications, since power lines could provide wired connection without requiring new infrastructure [3], [4], [5]. However, power line communication (PLC) poses many challenges [6]. Channel conditions depend on the local power network topology and on the devices plugged in nearby. Background noise levels are often high, noise is autocorrelated, and noise distributions are nonstationary and location-dependent [7]. Power-line attenuation and impedance vary with time and frequency [8], [9]. Electromagnetic compatibility regulations limit the signal power that a PLC system can inject into multiuse power lines.

Due in part to these challenges, the potential of PLC for smart grid applications remains largely unrealized. Addressing and ameliorating the challenges of the typically relatively poorly characterized PLC communication environment would open the door to effective dual use of the power line for communication and power delivery. Therefore, this article develops instrumentation that measures key variables in a local power distribution network. The resulting information–including the noise distribution, signal attenuation, and line impedance–makes it possible to tailor a PLC system to a current local power network environment. This article experimentally demonstrates that tailored PLC system communicates reliably where traditional PLC fails.

The key to unlocking the promise of PLC communication for energy control applications is instrumentation and measurement. Instrumentation tailored to the electric utility permits quick real-time characterization of power line conditions. Measurements can be taken once as a "commissioning" step for constructing a power delivery installation. They can also be taken repeatedly or continuously to characterize changes as new loads and utility conditions arise. This approach opens the door to "continuous commissioning," allowing a PLC system to adapt as necessary to ensure reliable communication [10]. This article describes custom hardware that can be used to characterize the main properties of a PLC channel. Results in this article demonstrate that three classes of information–measurements for noise floor, signal

Manuscript received 5 June 2022; revised 24 October 2022; accepted 18 November 2022. Date of publication 1 December 2022; date of current version 13 January 2023. This work was supported in part by The Exelon Corporation and in part The Grainger Foundation. The Associate Editor coordinating the review process was Dr. Jingyu Hua. *(Corresponding author: Adedayo O. Aderibole.)*

Adedayo O. Aderibole, Erik K. Saathoff, Aaron W. Langham, and Steven B. Leeb are with the Electrical Engineering and Computer Science Department, Massachusetts Institute of Technology, Cambridge, MA 02139 USA (e-mail: adedayo@mit.edu; saathoff@mit.edu; alangham@mit.edu; sbleeb@mit.edu).

Kevin J. Kircher is with the Mechanical Engineering Department, Purdue University, West Lafayette, IN 47907 USA (e-mail: kircher@purdue.edu).

Leslie K. Norford is with the Department of Architecture, Massachusetts Institute of Technology, Cambridge, MA 02139 USA (e-mail: lnorford@mit.edu).

Digital Object Identifier 10.1109/TIM.2022.3225916

attenuation, and line impedance–characterize a utility and permit rational decisions for configuring a PLC or an adaptive PLC installation. The custom instrumentation described in Section II can be used by a facilities manager or designer to plan a PLC installation. The hardware designs presented here can also be simplified and incorporated into products to permit loads to continuously adjust their communication interaction with other components on a local grid. To the best of our knowledge, a modular instrumentation device which can simultaneously characterize PLC channels and at the same time perform signaling has not been previously identified or explored in the existing literature. Furthermore, this article also presents a channel quality indicator (CQI) metric which directly relates the measured noise, attenuation, and impedance of a channel to its expected reliability. From the resulting CQI, this article shows how the measurements facilitate reliable real-time low-data-rate PLC using the same instrumentation device in challenging field locations. Results are demonstrated in two challenging test sites described in Section III: a U.S. Army microgrid for field operations and a 24-floor apartment building. While different, these two test sites make the point that most power systems can be thought of as "local" grids limited by critical components like generation on the Army microgrid, or a distribution transformer in the apartment building. These "local grids" are both effectively microgrids that benefit from coordinated load operation and information exchange. Experiments in Sections IV and V show how the instrumentation and measurement techniques developed in this article enable reliable communication at both test sites, including in situations where conventional "off-the-shelf" PLC systems fail.

II. PLC Modem and Test Instrumentation

This section describes the PLC modem and the instrumentation used to probe the current local channel conditions. This hardware is not intended for inclusion in every modem within a commercial PLC product. Rather, it could serve as a mobile test platform to aid the initial deployment, configuration, and commissioning of a PLC system within a new building, microgrid, or other environment.

The instrumentation hardware employed in this work includes a PLC modem with impedance estimation capability and a Raspberry Pi. Fig. 1 presents a top view of the PLC modem and Raspberry Pi. The PLC modem couples the transmitted or received carrier signal between the high-voltage power line and the low-voltage signal processing section with a multiple-input and multiple-output (MIMO) coupling circuit. The MIMO coupling circuit shown in Fig. 1 consists of transformers, solid-state relays, and capacitors. The low-voltage signal processing section make use of two Texas Instruments AFE032 analog front-ends (AFEs) for signal conditioning and a Cypress PSoC 5LP microcontroller (MCU) for discrete-time signal processing. The AFEs operate in the narrowband-PLC (NB-PLC) frequency band, between 3 and 500 kHz, and consist of configurable filters, a power amplifier (PA), and programmable-gain amplifiers (PGAs). The MCU configures the AFEs through a serial peripheral interface (SPI).

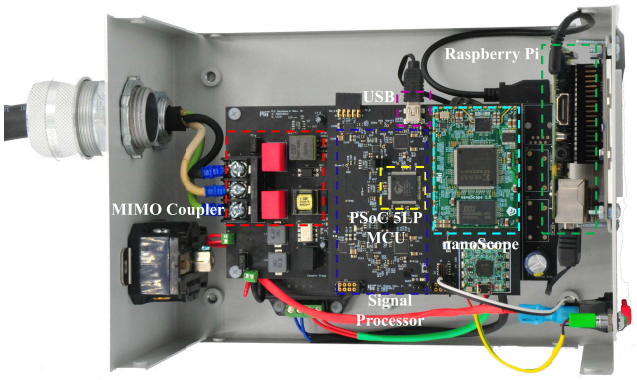

Fig. 1. Top view of the hardware including PLC modem and Raspberry Pi.

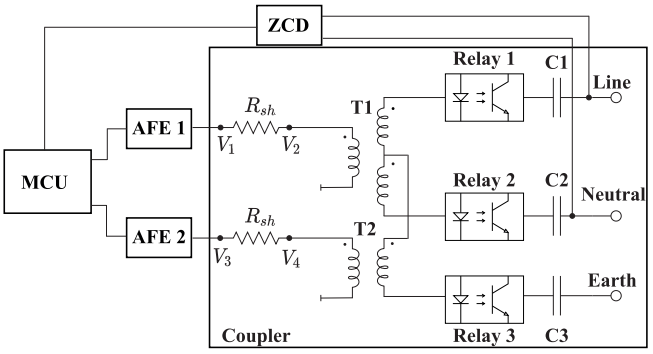

Fig. 2. Simplified circuit diagram of the developed PLC modem.

The instrumentation hardware shown in Fig. 1 facilitates the measurement of power-line noise, impedance, and attenuation required to enable effective PLC. A more detailed description and function of the hardware circuitry will be provided in Sections II-A–II-F.

A. Coupler

The MIMO coupler section of the circuit shown in Fig. 2 isolates the low-voltage circuitry from the high-voltage power line. The coupler also couples PLC signals between the AFEs and the power line during signal transmission and reception. The coupling circuit consists of transformers (T1 and T2), capacitors (C1, C2, and C3), solid-state relays (Relay 1, 2, and 3), and two shunt resistors. Both transformers, T1 (center-tapped) and T2 (noncenter-tapped), are manufactured by Wurth Electronics. The transformers possess low magnetizing and leakage inductance which ensure minimal coupling loss during signal transmission or reception. In addition to the transformers, three 0.47 μF metalized polypropylene capacitors (C1, C2, and C3) rated at 310 VAC safely isolate the low-voltage circuitry from the high-voltage power line. The capacitors block the high-voltage low-frequency AC mains voltage by presenting a 6.8 or 5.6-kΩ impedance at 50 or 60 Hz, respectively. The solid-state relays are rated for 400 V and are manufactured by Omron Electronics. The relays change the connection of the coupler to the electric utility, affecting the physical PLC channel. For instance, when only Relays 1 and 2 are closed, the line-neutral channel is being used. Closing all three relays enable full MIMO capability. The MCU controls the operation of the relays to select

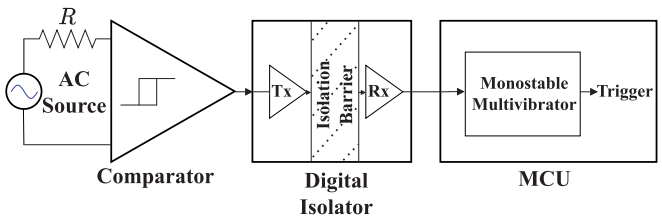

Fig. 3. AC mains voltage ZCD circuit.

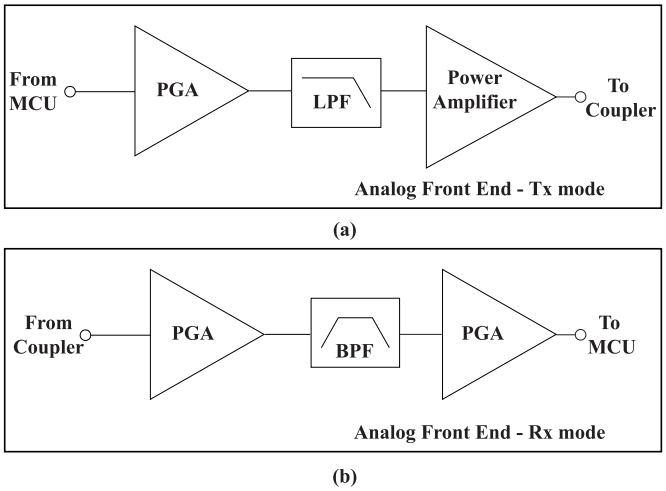

Fig. 4. AFE032 AFE circuit in (a) transmitter mode and (b) receiver mode.

appropriate physical channels used for signaling. The shunt resistors shown in Fig. 2 provide an avenue to estimate power-line impedance. Line-impedance measurements can be employed to develop sophisticated signaling schemes which adapt to varying PLC channel conditions. The developed hardware utilizes 0.05-Ω shunt resistors to estimate power-line impedance. Sections II-F and IV-C describe the procedure for estimating impedance.

B. Zero-Crossing Detector

The AC mains voltage provides a global clock to improve synchronization and timing between different PLC modems. The zero-crossing detection (ZCD) circuit, depicted in Fig. 3, converts the AC mains voltage to a digital voltage-polarity signal. In the ZCD circuit, the comparator first converts the AC voltage to a digital signal. After the comparator, a digital circuit isolates the low-voltage MCU from the high-voltage power line. An ultralow-power digital isolator manufactured by Skyworks Incorporated is used. In the MCU, a monostable multivibrator triggers on the rising edge of the digital isolator's output, signaling transmission or reception.

C. Analog Front-End

During signal transmission, before coupling, the carrier signal is conditioned in one or both of the AFEs. In transmit mode, the AFE032 AFE consists of a PGA, a low-pass filter (LPF), and a PA. Fig. 4(a) provides the circuit diagram of the AFE during signal transmission.

The MCU configures the AFE PGA gain, LPF cut-off frequency, and other parameters through a serial peripheral interface. The PGA boosts the carrier signal to an acceptable level for transmission. Configured by the MCU, the possible PGA gain settings are 1.15, 2.3, 3.25, and 4.6 V/V. Spurious signals emanating from the MCU and other components in the transmitter (Tx) can interfere with other radio devices operating within and outside the NB-PLC frequency spectrum. As a result, the LPF attenuates high-frequency signal components in the carrier. This low-pass filtering reduces out-of-band emissions. Accordingly, the unity-gain, fourth-order LPF present in the AFE032 AFE can be configured to have a cut-off frequency of 95, 150, 420, or 490 kHz. The LPF cut-off frequency, typically within the NB-PLC spectrum, should be higher than the largest information-bearing frequency component of the carrier signal. The final component in the transmit chain is the PA. The AFE032 chip implements the PA using a high-slew rate (75 V/μs), high-voltage (24 V), and high-current (3 A) operational amplifier (op amp). The PA provides linear gain of 7 V/V at its full-power bandwidth of 1 MHz. The PA enables efficient signal transmission through power lines with nonideal properties, including low-impedance and highly capacitive power lines.

In receiver mode, the AFE employs two high-performance PGAs and a very low-noise, unity-gain, fourth-order BPF to process the received signal in the analog domain. Fig. 4(b) illustrates the AFE circuit implementation in receiver mode. The MCU directly configures the PGAs and BPF through the serial peripheral interface. The first PGA amplifies or attenuates the signal from the coupler. The available gain settings of this PGA are 0.125, 0.25, 0.5, 1, 2, 4, 8, 16, and 32 V/V. Depending on the gain setting, the achievable bandwidth of the first PGA varies from 47 MHz (0.125 V/V) to 1.55 MHz (32 V/V). For applications with high noise or interference in the passband, configuring the PGA as an attenuator improves received signal integrity. The BPF attenuates out-of-band noise in the first PGA's output. The AFE032 chip implements the BPF by cascading a LPF and a high-pass filter (HPF). A second PGA can be employed to further amplify the filter output. The available gain settings of this PGA are 1, 4, and 16 V/V. The corresponding PGA bandwidths are 6.73, 5, and 3 MHz, respectively.

D. Microcontroller

The mixed-domain MCU modulates the bit stored in a Tx buffer into a continuous-time waveform. Fig. 5(a) presents the implementation of the low-data-rate PLC modulator. Two look-up tables (LUTs) store 8-bit discrete samples of the continuous-time waveforms that modulate bits. For instance, assume 150- and 180-kHz sinusoidal signals modulate "0" and "1" bits, respectively. In this case, the LUTs store 8-bit discrete-time samples of the 150- and 180-kHz sinusoidal signals. Depending on the bit to be transmitted, "0" or "1," samples of the carrier signal reach the digital-to-analog converter (DAC). The DAC transforms the 8-bit discrete-time sequence into its continuous-time equivalent. The implemented 8-bit DAC supports conversion at a maximum rate of 8 Msps and a full-scale output range from 0 to 4.08 V (16mV/bit). A PGA amplifies the continuous-time signal, while the analog MUX selects either AFE 1 or AFE 2 to further condition and amplify the signal.

Fig. 5(b) shows the PLC demodulator implemented in the MCU. An analog MUX selects either the signal from AFE 1 or

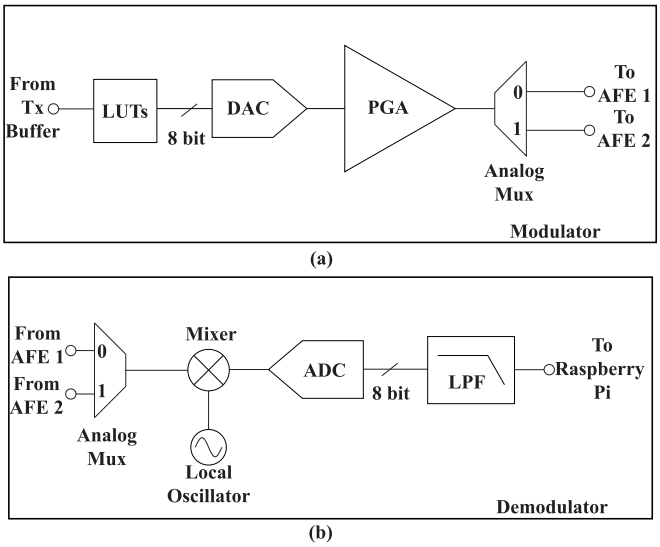

Fig. 5. Circuit diagrams of the (a) modulator and (b) demodulator implemented in the MCU.

AFE 2 for further processing. The selected AFE's output gets down-mixed to baseband by a mixer implemented in the MCU. An appropriate local oscillator (LO) frequency ensures the received signal gets shifted to baseband. For instance, LO frequencies of 150–190 kHz can be used to down-mix a 150-kHz sine wave for a 0–40-kHz baseband. Afterward, an analog-to-digital converter (ADC) converts the baseband signal from continuous-time to discrete-time. The discrete-time LPF after the ADC attenuates received signal components outside the baseband. As a result, the LPF cut-off frequency is selected to be slightly greater than the LO frequency. Finally, the MCU transfers the filtered received signal discrete-time samples to a Raspberry Pi through a USB interface.

E. NanoScope

If the ADC quantization becomes a limiting factor in the overall system noise, then it is advantageous to use a high-performance, dedicated ADC chip. The MCU is not well equipped to handle the high clock frequency and throughput, nor the digital signal processing on such a large bitstream. The nanoscope adds an alternative sampling and data processing route to the modem. This module consists of a multichannel ADC, FPGA, and SRAM. The ADC is an LT2325-16 four-channel, simultaneous sampling, 5 Msps, 16-bit ADC. The higher resolution and sampling rate substantially reduces quantization noise to obtain the cleanest possible signal. A Xilinx Spartan 3A FPGA runs the ADC at variable sampling rates up to 5 Msps. The four channels cannot be interleaved, but they can measure the same signal and average the result to increase the effective number of bits. ADC samples are streamed into an external 32 Mb (2M 16-bit words) SRAM. The FPGA communicates with the MCU through an SPI bus. This bus cannot handle the high data rates when the ADC is running at full speed, so the SRAM acts as a buffer. The FPGA also contains DSP resources, including three multipliers. These resources, coupled with the ability to form parallel pipeline processors, allow the FPGA to implement matched-filters and discrete Fourier transforms (DFTs) that run orders of magnitude faster than on the MCU.

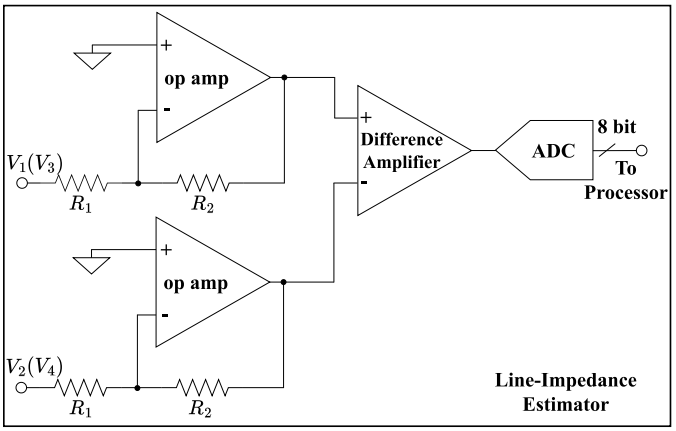

Fig. 6. Line-impedance estimator.

F. Impedance Estimator

Line impedance is a relevant parameter in the communication effectiveness of PLC modems. Drops in impedance near the carrier frequency tend to act as a signal sink, reducing the magnitude of the received signal. A common technique to measure line impedance is to inject a sinusoidal current into the line through a coupler and measure the associated voltage. Most of the components required for this measurement are already included in the PLC modem. The current measurement circuit shown in Fig. 6 is added to these components to enable impedance measurement. The circuit is also useful for determining the magnitude of current being injected into the line. The circuit measures the current through either R_{sh} resistor in the MIMO coupler. The circuit consists of two input inverting amplifiers, followed by a difference amplifier. An ADC in the MCU measures this difference voltage and converts it to current. By combining the voltage driven into the coupler by the AFE, the current measured by the MCU through the shunt resistor, and the properties of the coupler, the line impedance can be effectively measured. The procedure for this measurement is described further in Section IV-C.

III. Experiment Test Sites

This section describes the two test sites used for experimental validation of the instrumentation and measurement systems presented here. The first site, a military microgrid, can operate in either grid-connected or islanded mode. The microgrid's PLC channel characteristics change substantially between the two operating modes. The second site, a 24-floor apartment building, contains a large, diverse, and time-varying population of electrical loads, as well as multiple circuits and long runs of wire. Taken together, the two test sites present a wide variety of measurement and communication challenges.

A. Microgrid

The Future Capabilities Integration Laboratory (FCIL) located at Fort Devens, MA, USA, acts as a first case study for characterizing PLC channels. The FCIL is a microgrid utilized by the U.S. Army to rapidly evaluate future technologies and

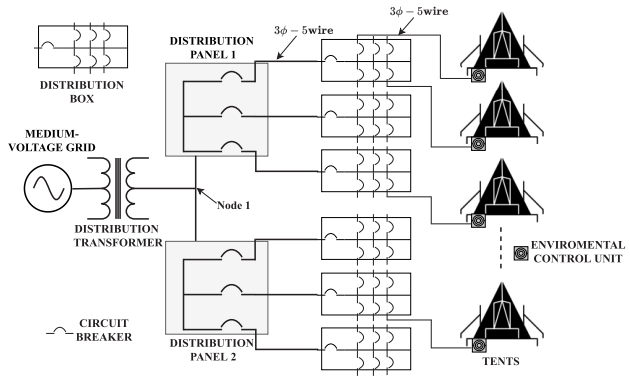

Fig. 7. Electrical circuit diagram of a military forward operating base operating as a grid-connected microgrid.

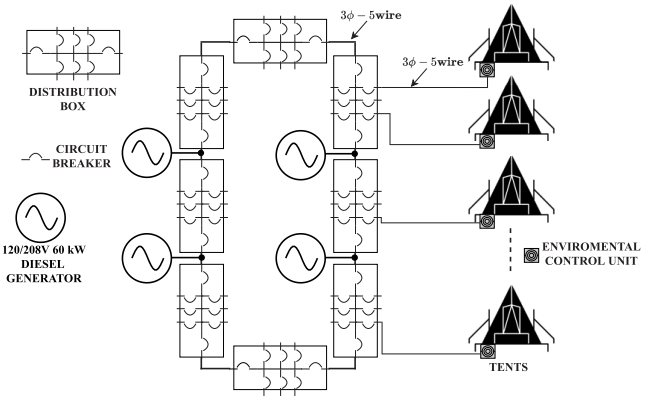

Fig. 8. Electrical circuit diagram of a military forward operating base operating as an islanded microgrid.

provide solutions to limit power demand in a forward operating base camp. The FCIL consists of tents and other systems that house and sustain soldiers in the field. The thermal environment in the tents is regulated by environmental control units (ECUs) to ensure occupant comfort. It was presented in [11] that due to the simultaneous operation of multiple ECUs in the FCIL, unfortunate and unnecessary peaks in aggregate power demand reduces operational reliability. Shabshab et al. [11] also showed that coordinating the ECUs can limit power demand in the forward operating base camp. As a result, the existing power lines in the FCIL can be leveraged to deploy PLC for facilitating ECU coordination. Therefore, the ability to measure PLC channel characteristics such as noise, impedance, and attenuation in the forward operating base camp enables the deployment of a reliable PLC system.

The FCIL microgrid operates in either grid-connected mode or islanded mode. The FCIL microgrid's electrical wiring system in the two modes of operation impacts PLC channel characteristics. Fig. 7 shows the electrical circuit diagram of the microgrid operating in grid-connected mode. When the FCIL microgrid operates in this mode, a distribution transformer delivers power from the utility grid to the microgrid. The neutral and earth conductors are bonded together at the transformer. Power supplied to the microgrid is split at node 1 to two distribution panels. Each panel distributes power to three different circuits through circuit breakers. Three-phase, five-wire cables deliver power from the two distribution panels to the six main circuits in the microgrid. Each main circuit has a portable power distribution box which splits the incoming power to six individual tents in the microgrid. For clarity, Fig. 7 only shows one distribution box delivering power to a maximum of two tents. The incoming power into each distribution box flows through a 200 A circuit breaker, while the outgoing power is delivered through either 60 A circuit breakers (four tents) or 100 A circuit breakers (remaining two tents). Other than the three-phase electrical outlet which delivers power to the ECU, each tent has multiple single-phase outlets used to power an array of other loads. The multiple circuit breakers in distribution boxes and panels attenuate PLC signals sharply when signals travel from one tent connected to a distribution panel to another tent connected to a different panel.

In islanded-mode, the FCIL microgrid is disconnected from the distribution transformer and powered by diesel generators. Fig. 8 presents the electrical circuit diagram of the islanded microgrid. A ring-bus configuration delivers power from the diesel generators to the tents. As shown in Fig. 8, the diesel generators feed power directly to the distribution boxes. The common ring bus formed by the distribution boxes allows PLC signals transmitted from one tent to be received in another tent. Each distribution box consists of two 200 A circuit breakers which can interrupt power supplied from either end of the distribution box. Similar to the distribution boxes in Fig. 7, power is delivered to the tents through 60 or 100 A circuit breakers. As a result, the multiple circuit breakers along the path traveled by PLC signals increase signal attenuation.

B. 24-Floor Apartment Building

The second test site is a 24-floor apartment building on the campus of the Massachusetts Institute of Technology. Electrical loads in this building, such as air conditioners and electric water heaters, can be controlled to enable building automation for demand response purposes. By equipping these loads with PLC modems, they can connect to the 24-floor apartment building's electrical system through the array of power outlets on various floors to create a local area network. This PLC network facilitates the communication of control commands for building automation. However, power-line noise, attenuation, and access impedance, which depend on the building's power distribution network, limit the reliability of PLC.

Fig. 9 illustrates the electrical system of the 24-floor apartment building. The three-phase, delta-wye grounded distribution transformer delivers power from the medium-voltage grid to the building. An air circuit breaker in the main service panel is used to provide overcurrent and short-circuit protection to the building's electrical circuit. Three-phase, four-wire cabling feeds power from the transformer to the main service panel, while three-phase, five-wire cabling supplies power from the main service panel to the two main circuits in the building. Fig. 9 shows that the earth and neutral conductors are bonded together at node 1. As indicated in Fig. 9, one main circuit supplies floors 2–13, while the other main circuit supplies floors 1 and 14 through 24. At nodes 3 and 4, the main circuits

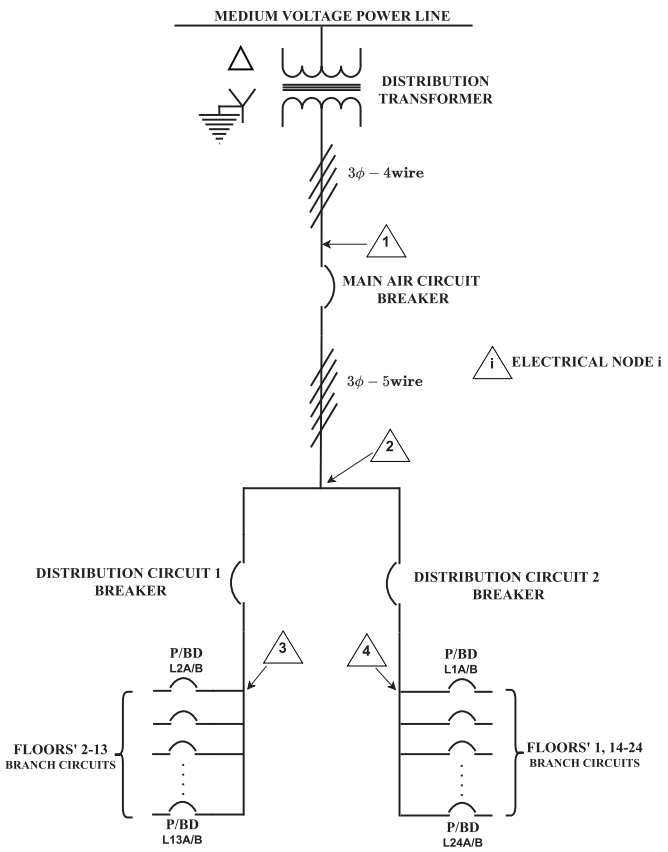

Fig. 9. Electrical circuit diagram of a 24-floor apartment building on the MIT campus.

branch to supply power to the individual floors. In addition to the distribution circuit breaker, two circuit breakers protect each floor's circuit. Single-phase and phase-phase electrical outlets in the apartments are supplied power from the floor's branch circuit three-phase, five-wire supply cables.

IV. Measurement and Discussion

This section presents procedures for measuring and characterizing power-line noise, attenuation, and impedance. As a case study, PLC channels in the FCIL microgrid described in Section III-A are characterized with instrumentation hardware presented in Section II. The resulting measurements of PLC channel attributes inform the proper design of reliable PLC systems and effective load control schemes.

A. Noise

Power-line noise in a facility occurs due to spurious emissions from electrical appliances (loads) such as switched-mode power supplies and light dimmers directly connected to the facility's electrical power system. For instance, in the FCIL microgrid described in Section III, as the conducted emissions from all the electrical appliances connected to the microgrid's electrical power system increase, so do the noise levels. As a result, accurate measurement of power-line noise environments can facilitate the deployment of reliable PLC for load control and demand response. Therefore, using the hardware shown in Fig. 1, this section presents instrumentation techniques employed to characterize power-line noise.

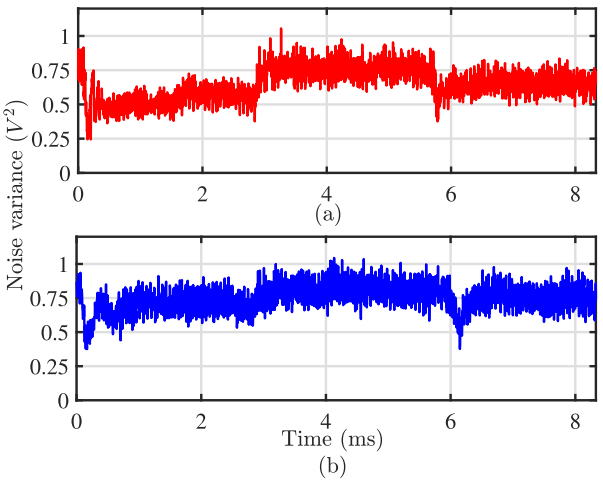

Fig. 10. Line-neutral power-line noise variance measured at an electrical outlet in the FCIL microgrid. (a) FCIL microgrid operating in grid-connected mode. (b) FCIL microgrid operating in islanded mode.

The hardware is used to obtain noise samples, $n(t)$ (V), from various PLC physical, temporal, and spectral channels. In this work, the AC line voltage acts as a clock to synchronize data acquisition. The circuit illustrated in Fig. 3 provides the clock signal which triggers data acquisition. As a result, the ADC triggered by the clock ensures the sampled data possess the correct time stamp relative to the AC line voltage positive zero crossing and stores the data in the correct order. The coupler circuit illustrated in Fig. 2 is configured to extract noise samples from the different physical channels. For example, to obtain noise samples from the line-neutral channel, Relays 1 and 2 are closed, while Relay 3 is open. The MCU selects the corresponding AFE, AFE 1 for the line-neutral channel, through the Analog Mux in Fig. 5(b). The MCU also configures the AFE by selecting appropriate gains for the PGAs and cut-off frequencies for the BPF. The LO frequency and LPF cut-off frequency in the MCU determine the frequency band occupied by the noise samples being acquired. In this study, the LO frequency is 210 kHz and the LPF cut-off frequency is 115 kHz. As a result, the noise samples transferred to the Raspberry Pi from the MCU occupy the 95–210-kHz frequency band. The hardware can be configured differently to obtain noise samples from a different physical or spectral channel. The output of the multivibrator in the MCU triggers the ADC in Fig. 5(b) to ensure the noise samples acquired are perfectly synchronized with the AC mains voltage cycle. This enables the characterization of the received noise data for the proper selection of PLC signal transmission time slots.

Figs. 10 and 11 present power-line noise variance measured in the FCIL microgrid. Fig. 10(a) and (b) plot the sample variance of noise obtained from the line-neutral physical channel when the microgrid operates in grid-connected mode and islanded mode, respectively. The sample variance was derived from two hundred noise observations synchronous with the AC mains voltage obtained from the 95–210-kHz spectrum. Power-line noise has an approximately Gaussian distribution with zero mean but nonstationary variance [12]. For zero-mean noise, variance corresponds to power. The noise

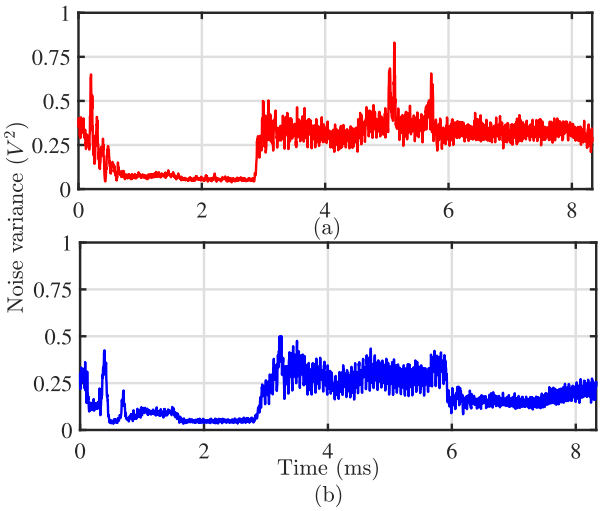

Fig. 11. Neutral-earth power-line noise variance measured at an electrical outlet in the FCIL microgrid. (a) FCIL microgrid operating in grid-connected mode. (b) FCIL microgrid operating in islanded mode.

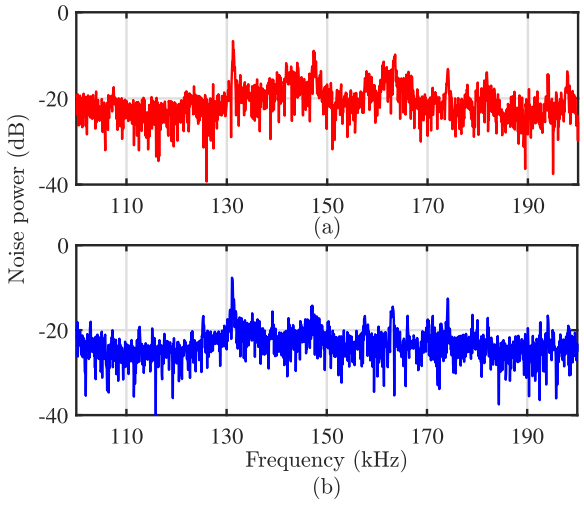

Fig. 12. Neutral-earth spectral noise power measured at an electrical outlet in the FCIL microgrid. (a) FCIL microgrid operating in grid-connected mode. (b) FCIL microgrid operating in islanded mode.

variance or power is typically periodic with a period equal to half that of the AC mains voltage. As a result, for a 60-Hz power system similar to the FCIL microgrid, the noise variance plotted in Fig. 10 has a period of 8.33 ms. By obtaining noise measurements with the hardware presented in this article, it can be seen in Fig. 10(a) that noise power is not constant. For instance, in Fig. 10(a), the overall noise power in the 0–3 ms time slot is lower than the overall noise power in the 3–6 ms time slot.

Fig. 11(a) and (b) plot the sample variance of noise obtained from the neutral-earth channel when the microgrid operates in grid-connected mode and islanded mode, respectively. Comparing Fig. 11 with Fig. 10 demonstrates that noise power is significantly less in the neutral-earth channel than in the line-neutral channel. This result suggests that communicating using the neutral-earth channel is more favorable than the line-neutral channel. In contrast to the PLC modem presented in Fig. 1, most commercially available PLC modems exclusively utilize the line-neutral physical channel for communication. As a result, in the FCIL microgrid, most commercial PLC solutions cannot leverage the more favorable noise environment in the neutral-earth physical channel to improve PLC performance. The ability to probe the different channels using the instrumentation hardware presented in Fig. 1 enables the detection of favorable PLC channels for signaling.

Existing low-bandwidth PLC protocols such as X10 and INSTEON exclusively employ the 0–1 ms time slot immediately after an AC mains positive zero-crossing for signal transmission [13]. However, observing Fig. 11(a) and (b) shows that noise power is lower in the 1–2 ms time slot than in the 0–1 ms time slot. The commercially available PLC modems operating with the X10 or INSTEON protocol are unable to leverage this variation in noise power over the AC mains voltage cycle to communicate using the 1–2 ms time slot instead of the 0–1 ms time slot for improved PLC performance. In contrast, similar to [10], the time-domain noise measurement procedure presented here facilitates the deployment of adaptive schemes that leverage the noise power variation to improve PLC performance.

Fig. 12 presents the spectral content of power-line noise measured in the FCIL microgrid. The DFT of the noise samples obtained from an electrical outlet in the FCIL microgrid is plotted to demonstrate the noise power in the frequency domain. For reliable PLC, communicating using frequency bands with lower noise power improves PLC performance. Fig. 12(a) and (b) plot the DFT of noise obtained from the neutral-earth physical channel when the microgrid operates in grid-connected mode and islanded mode, respectively. Except for narrowband noise at ≈131 kHz and other frequencies, it can be observed that the measured noise in the microgrid resembles white noise. Therefore, communicating at frequencies without narrowband noise suggests improved PLC performance. For example, consider the X10 and INSTEON low-bandwidth PLC protocols. The X10 protocol communicates using 120-kHz sine waves, while the INSTEON protocol communicates using 131.65-kHz sine waves [13]. The results in Fig. 12(a) and (b) suggest that the impact of noise will be higher for an INSTEON PLC system than an X10 PLC system. This is because of the narrowband noise with high power observed around 131 kHz in Fig. 12(a) and (b). Indeed, without observing the noise profile and adapting accordingly, it is impossible to know whether poor performance is the result of an unfortunately placed carrier frequency.

B. Attenuation

Unpredictable signal attenuation dependent on time of day, frequency, distance, and electrical phase deteriorates the received signal power in PLC systems [14]. Therefore, estimating PLC signal attenuation using instrumentation tools and adapting to the observed measurements can increase communication reliability.

In this work, PLC signal attenuation measurements in the FCIL microgrid are determined with the hardware shown in Fig. 1. In this test, a PLC modem connected to an electrical outlet in a tent transmits a known swept sinusoidal signal

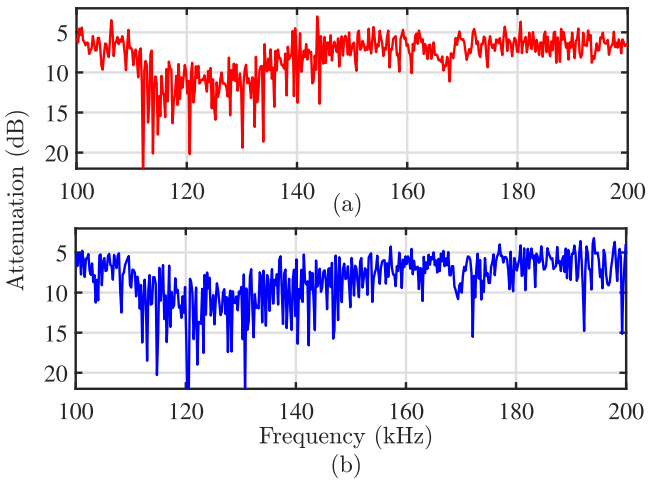

Fig. 13. Observed attenuation in FCIL microgrid. (a) FCIL microgrid operating in grid-connected mode. (b) FCIL microgrid operating in islanded mode.

to determine the attenuation on various PLC links in the microgrid. This swept sinusoidal signal has a duration of 4 ms and occupies the 100–200-kHz frequency band. At the other end of the PLC link, a receiver modem receives and stores samples of the received swept sinusoidal signal in the Raspberry Pi. Using the ZCD circuit, the AC mains voltage acts as a global clock to synchronize the Tx and receiver modems. From the DFTs of the transmitted, $x_T(f)$ in dB, and received, $x_R(f)$ in dB, swept sinusoidal signals, the PLC link attenuation is given by

$$\alpha(f) = x_T(f) - x_R(f) - n(f) \tag{1}$$

where $n(f)$ is the DFT of the noise at the receiver (in dB) and f denotes frequency.

Fig. 13(a) and (b) present the signal attenuation on the neutral-earth physical channel of a PLC link when the microgrid operates in grid-connected mode and islanded mode, respectively. This article only plots attenuation on the neutral-earth physical channel because attenuation on the line-neutral channels is too high to accurately estimate. This is because the presence of power electronics EMI filters tend to introduce a significantly higher capacitive load on the line-neutral channel [1]. Fig. 13 shows a pronounced increase in attenuation between 110 and 140 kHz. This means that PLC systems which communicate in this frequency band will experience higher signal attenuation than systems that communicate in other bands. For example, the X10 low-bandwidth PLC protocol communicates using the 120-kHz band [13]. The higher signal attenuation at this frequency will limit the performance of X10 PLC devices in the FCIL microgrid. An instrumentation and measurement survey which characterizes attenuation prior to system deployment can expose this limitation. Accordingly, for improved performance, the X10 protocol can be adapted to now communicate using 145-kHz sine waves.

C. Impedance

The line impedance measurement makes use of the AFE PA and the current shunt measurement circuit. The impedance

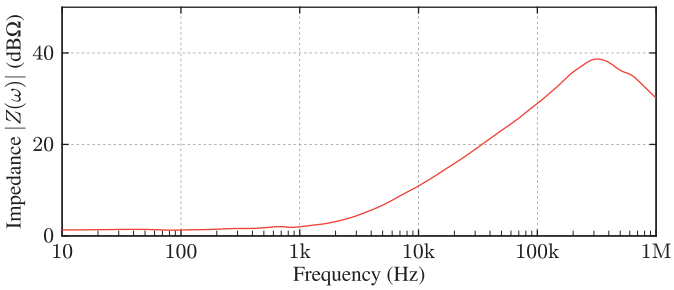

Fig. 14. Typical line-to-neutral impedance [15].

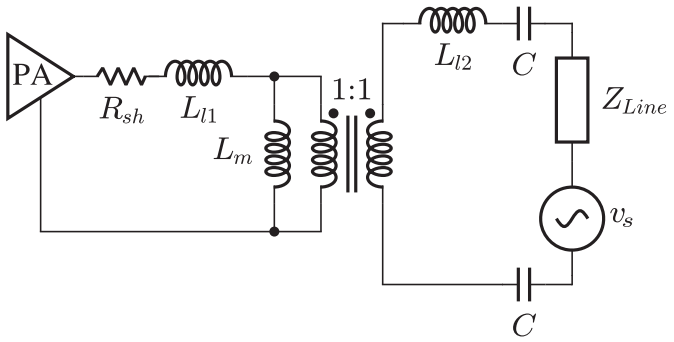

Fig. 15. Line-to-neutral impedance measurement configuration.

can be measured between any two power line conductors, but here we will consider the line-to-neutral impedance. Fig. 14 shows a typical line-to-neutral impedance measurement [15]. This measurement has been explored extensively, but usually requires an application specific circuit [8]. Here, the PLC hardware can be reused to measure line impedance. From Fig. 2, Relays 1 and 2 are closed, while Relay 3 is opened. In this configuration, only transformer T1 is in use and acts like a 1:1 transformer. Fig. 15 depicts this configuration when connected to the electric utility with the coupler components explored in more detail. R_{sh} is the current shunt resistor from the coupler in Fig. 2. Transformer T1 has been broken into four different pieces: L_{l1} and L_{l2} are the primary and secondary side leakage inductance, respectively, L_m is the primary side magnetizing inductance, and the ideal 1:1 transformer represents the turns ratio of T1. The upper and lower capacitors, C, are C_1 and C_2 of the coupler, respectively. The line is modeled as some AC voltage source v_s with series line impedance Z_{line}. This voltage source will exist regardless of the physical channel being probed. In the neutral-to-earth configuration, the voltage source is small and comes from voltage drops in the neutral conductor. This voltage source is not important, and will be attenuated by the high-pass characteristic of the coupler, and the signal processing on the measurement. When the AFE PA outputs a voltage sinusoid, there will be a resulting current that depends on the apparent impedance. Consider measurement frequencies high enough that the magnetizing inductance of the transformer is very large, the measured impedance Z_{meas} becomes

$$Z_{\text{meas}} = R_{sh} + j\omega L_l + \frac{2}{j\omega C} + Z_{\text{line}} \tag{2}$$

and

$$L_l = L_{l1} + L_{l2}. \tag{3}$$

The line impedance can be extracted by measuring the impedance looking into the coupler, and canceling the effects from known parameters. The procedure is relatively simple. First, a sinusoid at some magnitude, frequency ω_t, and phase is generated and sent out through the AFE. Then current through the shunt resistor is sampled. The MCU runs the sample current through a DFT calculation, but only at the fundamental frequency of the output sinusoid to find the current phasor. Finally, the voltage is divided by the current to determine $Z_{\text{meas}}(\omega_t)$. It is very important to keep track of when the AFE output updates, and when the current is sampled, to prevent timing errors related to conversion between analog and digital. The DFT is important as it will reject noise and harmonics in the voltage generated. This test can be completed over the desired frequency span and increment to build up the function Z_{meas}.

It is necessary to initially test with a known value of Z_{line}, such as a short circuit. In this case, the coupler must be disconnected from the electric utility and instead connected to a short circuit. By measuring over a range of frequencies, and assembling a least-squares tableau from various measurements, L_l and C can be accurately measured in circuit and include the effect of circuit parasitics. Components do not need to be measured before assembly, increasing the practicality for commercial use. The transformer leakage inductance is highly variable between parts, so this correction is crucial. Self calibration is possible if the short circuit is built into the board with an appropriate switch. The linearity between Z_{line} and Z_{meas} also means the effect of the coupler can be treated separately if $Z_{\text{coupler}}(\omega)$ is actually some arbitrary function. Z_{coupler} can be characterized and used as the offset between Z_{meas} and Z_{line}. This is helpful if there are unmodeled parasitics in the coupler, or if the coupler appears to have frequency dependent component values. The swept sine approach is reasonably resistant to nonlinearity, so these effects are manageable. Fig. 14 demonstrates power-line impedance. It can be seen that at low-bandwidth frequencies of interest, between 3 and 500 kHz, the power line acts as an inductor. Line-impedance measurements similar to the result published in Fig. 14 can be leveraged to select signal transmission frequencies and choose PLC couplers and PAs parameters for reliable PLC.

Due to the differences in PLC channel conditions in the various test locations, making a direct comparison of the results published in this article with results or methods presented in similar works such as [12], [14], [16], [17] becomes difficult. Notwithstanding, comparing the nature and pattern of the noise, attenuation, and impedance profiles presented in this work with the results published [12], [14], [16], [17] shows that the instrumentation and measurement techniques proposed in this article are able to capture the inherent nature of PLC channel characteristics.

D. Channel Quality Indicator

The PLC channel noise, attenuation and impedance can be further related to PLC reliability through the CQI. A PLC channel's reliability increases with its CQI. The CQI is related to the channel noise, attenuation, and impedance through

$$\text{CQI}(f,t) = \frac{Z_{\text{meas}}(f,t)}{n(f,t)\cdot\alpha(f,t)}(\Omega/V). \tag{4}$$

Equation (4) shows that the quality or reliability of a channel increases as the noise and attenuation decreases. Additionally, for higher access impedance, the ability to transfer more energy from the Tx to the power line increases which improves channel reliability. Therefore, condensing the measured noise, attenuation, and impedance into the CQI metric can inform the appropriate selection of channels for reliable low-data-rate PLC. Although the CQI metric is not directly related to the signal-to-noise ratio (SNR), both metrics depend on the channel noise and attenuation in the same way. For example, the lower the noise and attenuation, the higher the CQI and SNR. As a result, the CQI metric can provide important information about a PLC channel's reliability similar to the SNR. Furthermore, with the CQI, a PLC channel's reliability can be estimated using a simple instrumentation and measurement device in the absence of an actual PLC modem.

As an illustration, consider the neutral-earth channel in the FCIL microgrid characterized in Sections IV-A–IV-C. Comparing the noise in the 120 and 131.5 kHz channels in Fig. 12 shows higher noise levels in the 131.5 kHz compared to the 120 kHz. Figs. 13 and 14 demonstrate similar attenuation and impedance levels in both the 120 and 131.5 kHz channels. Due to the lower noise experienced in the 120 kHz channel, it can be deduced that the 120 kHz channel possess a higher CQI than the 131.5 kHz which leads to higher reliability.

In this work, measurement errors typically arise from the DFT implementation, amplifiers, ADC, and DAC. Therefore, during the noise, attenuation, or impedance measurement process, errors introduced at various points add uncertainty to the final measurement. This article primarily aims to select an appropriate PLC channel for signaling by comparing the reliability of different potential PLC channels. By assuming the individual measurement errors remain constant, the impact of errors on the measured CQI for one channel with respect to the other channels nullifies one another.

V. PLC Field Test Results

This section evaluates the reliability of low-data-rate PLC in the microgrid and apartment building described in Section III. The presented results demonstrate how the ability to measure key PLC channel attributes facilitates the deployment of effective PLC. For the microgrid field test, the ability of the proposed instrumentation hardware to facilitate the selection of reliable physical channels (line-neutral versus neutral-earth) using offline measurements is analyzed. For the apartment building field test, noise variance measurements in the time domain inform the selection of reliable time slots for low-data-rate signaling.

A. Microgrid Field Test

In these tests, a PLC modem connected to an electrical outlet in a tent, denoted as Tent 1, transmits a known symbol (bit) sequence to determine the reliability on various PLC

links. The reliability on the different PLC links is tested when the microgrid operates in grid-connected mode and islanded mode. In grid-connected mode, a receiver modem is connected to an electrical outlet in three tents, Tents 2–4, to decode the transmitted bit sequence. In this test, Tent 1 (the Tx location) and Tent 2 are connected to the same distribution panel and portable power distribution box. Tents 1 and 3 are connected to the same distribution panel but different portable power distribution box. Finally, Tents 1 and 4 are connected to different distribution panels. This diverse location of the receiver modems builds confidence in the field tests' ability to demonstrate low-data-rate PLC performance throughout the microgrid.

In the islanded mode of operation, the Tx modem remains in Tent 1. Now, the receiver modem is connected to an electrical outlet in only two tents: Tents 2 and 3. Tents 1 and 2 are connected to the same power distribution box, while Tent 3 is connected to a different distribution box. There are no distribution panels when the microgrid operates in islanded mode.

In this field demonstration, the 150–180-kHz spectral channel is used for communication. The chirp spread spectrum signaling scheme proposed in [1] is employed for modulation and demodulation. This scheme leverages the time-frequency characteristics of chirp signals and the quasi-peak regulations to increase transmitted power in the 150–500-kHz band [1]. The chirp signals used to modulate transmitted data have a duration of 1 ms. The reliability of the PLC links is tested on both the line-neutral and neutral-earth channels. Section IV already shows higher noise and attenuation measurement in the line-neutral channel versus the neutral-earth channel. As a result, the CQI of the neutral-earth channel can be inferred to be lower than the CQI of the line-earth channel. Therefore, for reliable low-data-rate PLC, the microgrid can be commissioned to communicate using the neutral-earth channel instead of the line-neutral channel. Without this information derived from the instrumentation hardware presented in this article, an opportunity to achieve reliable PLC using the neutral-earth channel could have been missed in the microgrid. Results in this section validate this claim.

Fig. 16 demonstrates the reliability of the FCIL microgrid's neutral-earth PLC links when operating in grid-connected mode. In this case, the Tx is placed in Tent 1. Fig. 16 shows that the reliability of the Tents 1–2 and Tents 1–3 PLC links are high. On these links, a one-hundred percent detection probability is achieved for 12 symbols (bits)/s or less data rates. For the Tents 1–4 link, it can be observed that PLC reliability worsens. A one-hundred detection probability can only be achieved at 9 symbols/s. The reduction in PLC link reliability results from the increased attenuation experienced by PLC signals traveling through the extra circuit breakers in the microgrid's distribution panels when communicating from Tents 1 to 4. Regardless of this increased attenuation, Fig. 16 shows that reliable low-data-rate PLC can be achieved in the FCIL microgrid when using the neutral-earth channel for signaling.

Due to the excessive signal attenuation and noise levels in the FCIL microgrid's line-neutral channel, the detection

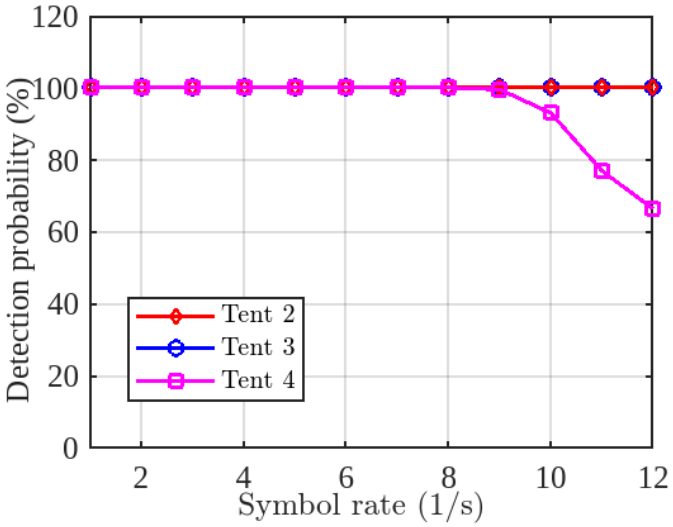

Fig. 16. Reliability of neutral-earth PLC links in the FCIL microgrid when operating in grid-connected mode.

probabilities on all the tested line-neutral links were observed to be zero percent although not shown in Fig. 16. Therefore, many existing PLC modems designed to only communicate using the line-neutral channel limit their efficacy in a difficult environment similar to the FCIL microgrid. This limitation was further validated after testing the reliability of an off-the-shelf PLC modem which only employs the line-neutral channel for communication [18]. In addition to only using the line-neutral channel, this off-the-shelf modem communicates using 131.8 and 133.3 kHz sine waves. Due to the higher signal attenuation and overall noise power in the line-neutral channel, this traditional PLC modem fails to reliably communicate in the microgrid. This traditional modem would potentially perform more effectively if measurements of noise and other parameters in the available physical, spectral, and temporal channels decided system configuration. Using the CQI metric and the instrumentation hardware described in this article, this could have been predicted during PLC system design.

Fig. 17 demonstrates the reliability of the FCIL microgrid's neutral-earth links when operating in islanded mode. Published results show that a one-hundred percent PLC reliability can be achieved on the Tents 1–2 and Tents 1–3 links at 12 symbols/s or less data rates. However, the line-neutral links still remain unreliable. This confirms that the hardware shown in Fig. 1 can facilitate the design of a reliable low-data-rate PLC system in the FCIL microgrid, regardless of its operation mode.

B. Apartment Building Field Test

In this test, the noise power estimated by the instrumentation hardware in the time domain informs transmission time slot selection for improved PLC reliability in the apartment building already described in Section III-B. Fig. 18 shows noise power (variance) measured in the apartment building similar to Figs. 10 and 11 for the FCIL microgrid. Assuming one ms long symbols, this noise power variation in the time domain suggests that signaling in the 6–7 ms (slot 7) time slot could be more reliable than signaling in the 0–1 ms (slot 1) time slot. This is because of the lower noise power in the

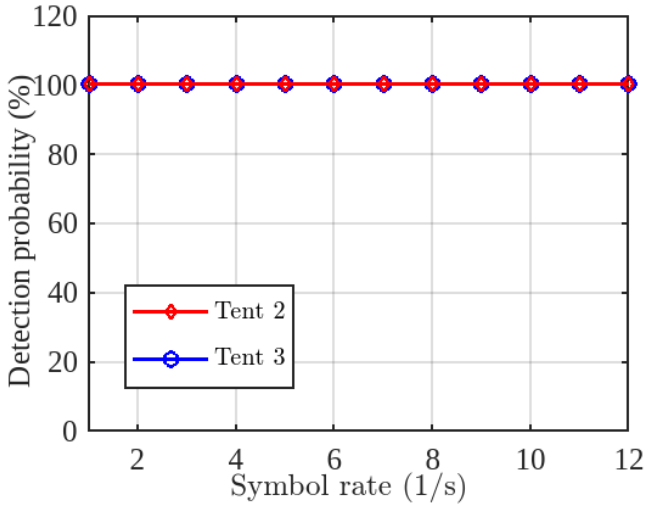

Fig. 17. Reliability of neutral-earth PLC links in the FCIL microgrid when operating in islanded mode.

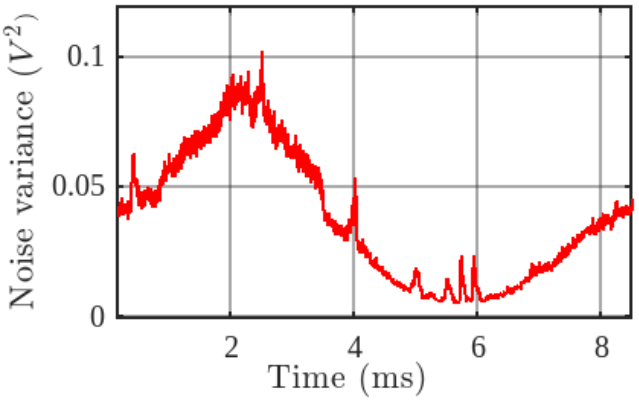

Fig. 18. Neutral-earth power-line noise variance measured at an electrical outlet in the apartment building.

6–7 ms time slot which can be determined during a one-time or continuous commissioning of the PLC system using the presented instrumentation hardware.

Fig. 19 compares PLC reliability in the apartment building when signaling in the 6–7 ms (seventh) time slot versus the 0–1 ms (first) time slot. In this test, the receiver is located on the 24th floor and the Tx is placed on either the 14th or 18th floor. The solid lines depict the seventh time slot case, while the dashed lines denote the first time slot case. Compared to the first time slot, Fig. 19 shows that transmitting and detecting signals using the seventh time slot improves reliability of the 14th–24th and 18th–24th PLC links. Using the seventh time slot achieves detection probability of 100% at five and 6 symbols/s in the 14th–24th and 18th–24th PLC links, respectively. However, using the first time slot can only provide detection probability of 66% at 5 symbols/s for the 14th–24th PLC link and 60% at 5 symbols/s for the 18th–24th PLC link. This performance disparity is due to the higher noise power in the first time slot compared with the seventh time slot. Many existing low-data-rate PLC protocols including INSTEON and X10 always communicate using the first time slot. However, Figs. 18 and 19 suggests this does not always maximize signaling reliability. Therefore, the ability to measure noise

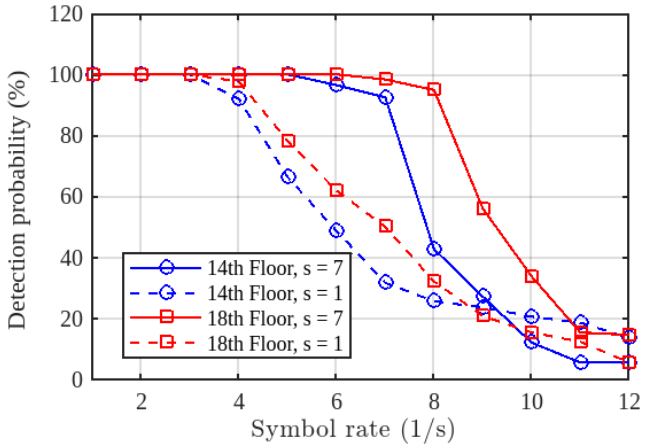

Fig. 19. Reliability of different time slots with different noise power. The PLC Tx is located on the 14th and 18th floor, while the receiver is located on the 24th floor.

power using the proposed instrumentation hardware and select appropriate time slots enables the commissioning of reliable signaling. Aderibole [10] further explores more sophisticated algorithms which periodically adapt signaling to changing noise power for continuous commissioning of a reliable PLC system.

Although increasing the transmitted signal power typically improves communication reliability, regulatory bodies limit the amount of power that can be transmitted to reduce conducted and radiated emissions [1]. Therefore, in a challenging environment similar to the 24-floor apartment building, increased reliability can sometimes only be achieved by adapting to the measured channel characteristics when already transmitting at maximum power. For example, Fig. 19 achieves this by transmitting in slot 7 instead of slot 1 because of its lower measured noise power which translates to increased reliability. This increased reliability is achieved even though the PLC Tx operates at maximum power in both cases.

VI. Conclusion

Upon reflection, it is something of a miracle that commercial, off-the-shelf PLC systems are able to communicate at all in as many situations as they do. Inevitably, power connections and wiring will vary, and applications of PLC for professional applications with more guaranteed performance require a more formal approach for installation and application. Proper instrumentation and measurement permit characterization of local electric utility connections to find openings for reliable PLC communication. Power line measurements can be used to configure PLC for best-available performance, and also to adapt PLC systems to changing conditions.

This article has presented a suite of instrumentation that measures key variables within a section of a power distribution system. These measurements enable tuning of PLC system parameters to the current local channel conditions. A range of experiments in a microgrid as well as a 24-floor apartment building have validated the effectiveness of the instrumentation suite. Experiments have also shown that after measurement-enabled parameter tuning, the PLC system described here communicates reliably where traditional PLC systems fail.

ACKNOWLEDGMENT

The authors gratefully acknowledge the support of William Singleton, Jeffrey Gladney, and Robin Szczuka at the Future Capabilities Integration Laboratory, Fort Devens, MA, USA.

REFERENCES

[1] A. O. Aderibole, E. K. Saathoff, K. J. Kircher, S. B. Leeb, and L. K. Norford, "Power line communication for low-bandwidth control and sensing," *IEEE Trans. Power Del.*, vol. 37, no. 3, pp. 2172–2181, Jun. 2021.

[2] A. O. Aderibole, K. J. Kircher, S. B. Leeb, and L. K. Norford, "Distributed load control using reliable low-data-rate power line communication," *IEEE Access*, vol. 10, pp. 50242–50253, 2022.

[3] C.-H. Lien, H.-C. Chen, Y.-W. Bai, and M.-B. Lin, "Power monitoring and control for electric home appliances based on power line communication," in *Proc. IEEE Instrum. Meas. Technol. Conf.*, May 2008, pp. 2179–2184.

[4] G. Artale et al., "A new low cost power line communication solution for smart grid monitoring and management," *IEEE Instrum. Meas. Mag.*, vol. 21, no. 2, pp. 29–33, Mar. 2018.

[5] G. Artale et al., "Implementation of a PLC field analyzer on a G3 modem platform," in *Proc. IEEE Int. Instrum. Meas. Technol. Conf. (IMTC)*, May 2021, pp. 1–6.

[6] E. Biglieri, "Coding and modulation for a horrible channel," *IEEE Commun. Mag.*, vol. 41, no. 5, pp. 92–98, May 2003.

[7] H. Gassara, F. Rouissi, and A. Ghazel, "A novel stochastic model for the impulsive noise in the narrowband indoor PLC environment," in *Proc. IEEE Int. Instrum. Meas. Technol. Conf. (IMTC)*, May 2015, pp. 62–67.

[8] G. Hallak, C. Nieß, and G. Bumiller, "Accurate low access impedance measurements with separated load impedance measurements on the power-line network," *IEEE Trans. Instrum. Meas.*, vol. 67, no. 10, pp. 2282–2293, Oct. 2018.

[9] G. Artale et al., "A line impedance calculator based on a g3 plc modem platform," *IEEE Trans. Instrum. Meas.*, vol. 71, pp. 1–10, 2022.

[10] A. O. Aderibole, "Power line communication for low-data-rate energy control," Ph.D. dissertation, Dept. Elect. Eng. Comput. Sci., Massachusetts Inst. Technol., Cambridge, MA, USA, 2022.

[11] S. C. Shabshab et al., "Demand smoothing in military microgrids through coordinated direct load control," *IEEE Trans. Smart Grid*, vol. 11, no. 3, pp. 1917–1927, Oct. 2020.

[12] M. Katayama, T. Yamazato, and H. Okada, "A mathematical model of noise in narrowband power line communication systems," *IEEE J. Sel. Areas Commun.*, vol. 24, no. 7, pp. 1267–1276, Jul. 2006.

[13] P. Darbee, "Insteon developer's guide," SmartLabs Technol., San Francisco, CA, USA, Tech. Rep., Aug. 2007.

[14] M. H. L. Chan and R. W. Donaldson, "Attenuation of communication signals on residential and commercial intrabuilding power-distribution circuits," *IEEE Trans. Electromagn. Compat.*, vol. EC-28, no. 4, pp. 220–230, Nov. 1986.

[15] E. K. Saathoff, S. R. Shaw, and S. B. Leeb, "Line impedance estimation," *IEEE Trans. Instrum. Meas.*, vol. 70, pp. 1–10, 2021.

[16] R. M. Vines, H. J. Trussell, K. C. Shuey, and J. B. O'Neal, "Impedance of the residential power-distribution circuit," *IEEE Trans. Electromagn. Compat.*, vol. EMC-27, no. 1, pp. 6–12, Feb. 1985.

[17] R. M. Vines, H. J. Trissell, L. J. Gale, and J. B. O'neal, "Noise on residential power distribution circuits," in *IEEE Trans. Electromagn. Compat.*, vol. EMC-26, no. 4, pp. 161–168, Nov. 1984.

[18] *Cypress High Voltage Programmable Powerline Communication Development Kit Guide*, CY3274 Datasheet, Cypress, San Jose, CA, USA, 2014.

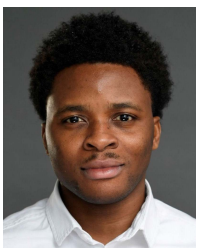

Adedayo O. Aderibole received the B.Sc. degree in electronic/electrical engineering from Obafemi Awolowo University, Ile-Ife, Nigeria, in 2013, the M.Sc. degree in electrical power engineering from the Masdar Institute, Khalifa University of Science and Technology, Abu Dhabi, UAE, in 2017, and the Ph.D. degree in electrical engineering and computer science from Massachusetts Institute of Technology, Cambridge, MA, USA, in 2022.

His research interests include communication theory, signal processing, and power system modeling and control.

Erik K. Saathoff (Graduate Student Member, IEEE) received the B.S. degree in electrical engineering with a minor in physics from the University of Illinois at Urbana-Champaign, Urbana, IL, USA, in 2018, and the M.S. degree in electrical engineering and computer science from the Massachusetts Institute of Technology, Cambridge, MA, USA, in 2021, where he is currently pursuing the Ph.D. degree in electrical engineering and computer science.

His research interests include high-performance power electronics, switched-capacitor converters, and system identification.

Kevin J. Kircher (Member, IEEE) received the Ph.D. degree in mechanical engineering from Cornell University, Ithaca, NY, USA, in 2019.

He has been an Assistant Professor of Mechanical Engineering at Purdue University, West Lafayette, IN, USA, since 2022. He develops optimization, control, and machine learning methods for energy systems in buildings, focusing on their interaction with the power grid. Before Purdue University, he was a Post-Doctoral Researcher in electrical engineering and computer science at the Massachusetts Institute of Technology, Cambridge, MA, USA.

Aaron W. Langham (Graduate Student Member, IEEE) received the B.E.E. degree in electrical engineering from Auburn University, Auburn, AL, USA, in 2018, and the M.S. degree in electrical engineering and computer science from the Massachusetts Institute of Technology, Cambridge, MA, USA, in 2022, where he is currently pursuing the Ph.D. degree in electrical engineering and computer science.

His research interests include signal processing and machine learning for energy management.

Leslie K. Norford received the Ph.D. degree in mechanical and aerospace engineering from Princeton University, Princeton, NJ, USA, in 1984.

After five years of active duty as a nuclear power officer in the U.S. Navy. He has been a Member of the Faculty of the Department of Architecture at the Massachusetts Institute of Technology, Cambridge, MA, USA, since 1988. His research interests include design, operation, and fault detection of space conditioning systems for low-carbon buildings and interactions of buildings with the electrical grid and with urban environments.

Steven B. Leeb (Fellow, IEEE) received the Ph.D. degree from the Massachusetts Institute of Technology, Cambridge, MA, USA, in 1993.

He has served as a Commissioned Officer for the United States Air Force (USAF) reserves, and he has been a member of the Massachusetts Institute of Technology (MIT) Faculty at the Department of Electrical Engineering and Computer Science, since 1993. He also holds a joint appointment in MIT's Department of Mechanical Engineering. He is the author or coauthor of over 200 publications and 20 U.S. patents in the fields of electromechanics and power electronics.